applied sciences

MDPI

Article

Computational Design of a Novel Dithranol–Salicylic Acid Antipsoriatic Prodrug for Esterase-Activated Topical Drug Delivery

Natália Andrýsková [1], Jozef Motyčka [2,3], Melánia Babincová [3], Peter Babinec [3,*] and Mária Šimaljaková [1]

[1] Department of Dermatovenereology, Faculty of Medicine, Comenius University and Bratislava University Hospital, Mickiewiczova 13, 813 69 Bratislava, Slovakia; babincova15@uniba.sk (N.A.); maria.simaljakova@sm.unb.sk (M.Š.)
[2] Department of Pharmaceutical Analysis and Nuclear Pharmacy, Faculty of Pharmacy, Comenius University Bratislava, Odbojárov 10, 832 32 Bratislava, Slovakia; jozef.motycka@uniba.sk
[3] Department of Nuclear Physics and Biophysics, Faculty of Mathematics, Physics and Informatics, Comenius University, Mlynská dolina F1, 842 48 Bratislava, Slovakia; babincova@fmph.uniba.sk
* Correspondence: babinec@fmph.uniba.sk

Abstract: Psoriasis is a chronic autoimmune skin disorder characterized by the rapid overproduction of skin cells, resulting in the formation of red, inflamed, and scaly patches or plaques on the skin. Dithranol, also known as anthralin, is a very effective topical medication used in the treatment of psoriasis, with several shortcomings like photo-instability; staining skin, clothing, and bedding; and causing skin irritation. Antiproliferative dithranol is frequently used in combination therapy with keratolytic salicylic acid. We have therefore proposed a novel topical antipsoriatic prodrug comprising dithranol and salicylic acid joined together with an ester bond, specifically 8-hydroxy-9-oxo-9,10-dihydroanthracen-1-yl-2-hydroxybenzoate. An ester bond is cleavable by endogenous esterase hydrolyzing this bond and releasing dithranol and salicylic acid in a 1:1 stoichiometric ratio. We performed an exhaustive theoretical analysis of this molecule using the reliable computational methods of quantum chemistry and ADME in silico studies to investigate its biological and pharmacokinetic activities. We found its molecular structure, vibrational spectra, molecular orbitals, MEP (molecular electric potential), UV-VIS spectra, and TDOS (total density of states), and we performed an RDG (reduced density gradient) analysis. The obtained results may be useful for the understanding of its properties, which may assist in the synthesis and further experimental study of this possible antipsoriatic dual-action prodrug with reduced adverse effects and enhanced therapeutic efficacy.

Keywords: psoriasis; dithranol; salicylic acid; ester bond; prodrug; quantum chemistry; molecular structure

Citation: Andrýsková, N.; Motyčka, J.; Babincová, M.; Babinec, P.; Šimaljaková, M. Computational Design of a Novel Dithranol–Salicylic Acid Antipsoriatic Prodrug for Esterase-Activated Topical Drug Delivery. *Appl. Sci.* **2024**, *14*, 1094. https://doi.org/10.3390/app14031094

Academic Editors: Gianpiero Calabrese and Antonia Mancuso

Received: 4 January 2024
Revised: 23 January 2024
Accepted: 25 January 2024
Published: 27 January 2024

1. Introduction

Psoriasis is a multifactorial immune-mediated systemic disease with a number of comorbidities [1–8]. The exact cause of psoriasis, which affects about 150 million people worldwide, is not fully understood. The genetic component plays an important role. Its heredity component is polygenic or multifactorial. The disposition to the disease (psoriatic diathesis, latent psoriasis) is inherited, not the disease itself.

Due to its relatively high prevalence in the population, its chronic course, and the significant percentage of severe forms, it is one of the most pharmacoeconomically demanding diseases.

The key features of psoriasis are

1. Red patches: the affected areas of the skin are red and inflamed.
2. Silvery scales: overlying the red patches, there are often silvery or white scales.

3. Itching and discomfort: psoriasis plaques can be itchy, and the skin may feel sore or painful.
4. Nail changes: psoriasis can also affect the nails, causing changes such as pitting, discoloration, and separation from the nail bed.

Psoriasis therapeutic modes include:

1. Topical treatments: these include corticosteroid creams, vitamin D analogues, retinoids, dithranol, coal tar, and moisturizers.
2. Phototherapy: exposure to ultraviolet light can be beneficial for some individuals with psoriasis.
3. Systemic medications: In cases of moderate-to-severe psoriasis, oral or injectable medications (e.g., methotrexate) can be used.
4. Biologics: these are a newer class of medications that target specific components of the immune system involved in the development of psoriasis (e.g., IL 12/23 blocker–ustekinumab and anti-IL-17–secukinumab).

The development of effective local treatments involves not only the discovery of new therapeutic substances but also advancements in the formulation or preparation of these substances [9–11].

One of the most successful drugs used in treatment of psoriasis is dithranol (Figure 1), also called anthralin [12–19], routinely used since 1916 [18], but the antipsoriatic effect of chrysarobin, the precursor of dithranol, a substance of plant origin, was described as early as 1876 by Squire. Dithranol (DIT) inhibits the synthesis of DNA that hyperproliferates the epidermis, adjusts the cycle of epidermal renewal, suppresses the production of products of the arachidonic acid cascade, suppresses the penetration of neutrophils into the epidermis, limits the activation of lymphocytes and the function of dendritic cells in target cells, acts at the level of mitochondria, and thus has several desired effects precisely in the psoriatic process [20]. The combination of dithranol with sub-erythemal doses of UVB (an amount of UVB that is insufficient to cause erythema–skin reddening, which is a measure of the amount of UVR that penetrates the skin without causing any visible damage) is the principle of the so-called Ingram treatment. The manifestations are freed of scales, irradiated with a UVB lamp, and then accurately treated with dithranol in a trap or ointment. Its initial concentration is 0.1%, with a gradual increase in concentration to 4 percent if the skin's reaction allows. This procedure is repeated after 18 to 22 h. Most patients recover within 3 weeks [21,22].

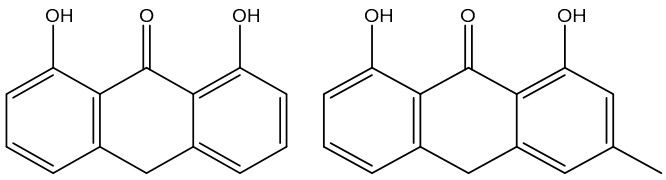

Dithranol **Chrysarobin**

Figure 1. Chemical structures of dithranol (1,8-dihydroxyanthracen-9(10H)-one) and chrysarobin (1,8-dihydroxy-3-methylanthracen-9(10H)-one).

Unpleasant brown–violet coloration [23] and skin irritation due to the formation of dithranol metabolites such as danthron and bianthrone (Figure 2) at the application site formed upon the exposure of dithranol to atmospheric oxygen are the main reasons for its limited usage [24–28]. It cannot be applied to the area of the head and neck, the bends of large joints, or the external genitalia.

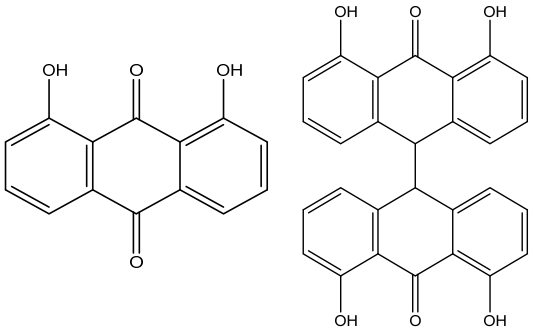

Figure 2. Chemical structures of main degradation products of dithranol: danthron (1,8-dihydroxyanthracene-9,10-dione) and bianthrone (4,4′,5,5′-tetrahydroxy-[9,9′-bianthracene]-10,10′(9H,9′H)-dione).

Dithranol itself is derived from chrysarobin [29]; therefore, it is not surprising that some efforts have been directed towards the improvement of the therapeutic index of dithranol by attempting to separate the beneficial effects from the side effects of the drug. This has been realized by the development of new derivates [30–33], where the staining effect of the drug would be at least theoretically reduced (Figure 3).

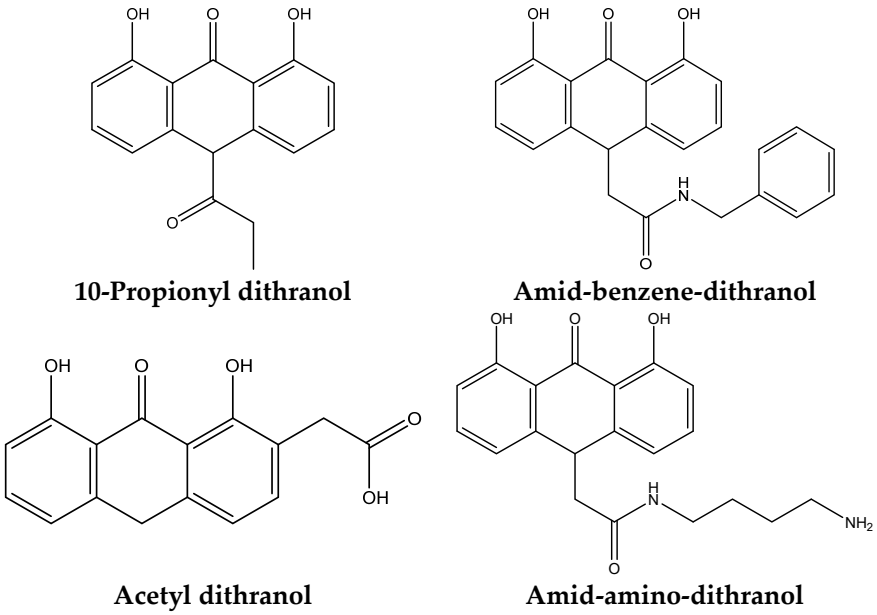

Figure 3. Chemical modifications of dithranol, proposed as a possible new antipsoriatic drug.

The ability of dithranol to induce keratinocyte differentiation was investigated and correlated with its potency to inhibit the proliferation of keratinocytes [34,35]. To determine the structural requirements for this effect, dithranol and 17 analogues or related anthracenones were examined for their ability to induce the formation of the cornified envelope (a marker of terminal differentiation). Moreover, dithranol, dithranol dimer, and dithranol triacetate exhibited antiproliferative and antirespiratory activity at concentrations required to induce keratinocyte differentiation, suggesting causality between these effects. In addition, cornified envelope formation was observed for several related anthracenones at low concentrations. In general, compounds containing benzoyl substituents, independent of their position in the anthralin nucleus, were more potent than those with benzyl substituents. The basic principles include combined treatment. The idea is to increase the efficiency and decrease the adverse effects of the treatment. This combination of drugs is not accidental but arises from pathogenesis diseases, where it is necessary to

suppress both immunopathological inflammation and, on the other hand, a disorder of differentiation and apoptosis. In most therapeutic regimes, dithranol is combined with salicylic acid [17,28]. Salicylic acid is an important ingredient in many skin products that treat acne, psoriasis, corns, keratosis pilaris, and warts, utilizing its keratolytic, analgesic, antibacterial, and anti-inflammatory properties [36]. It is advantageous if combination therapy can be administered in the form of a prodrug, where two drugs working against the same condition are joined by a cleavable covalent bond. Examples of prodrugs based on the enzymatic hydrolysis of ester bond-activated drug release are rather common, e.g., procaine, simvastatin, and enalapril [37,38].

The dithranol hydroxyl –OH moiety and the complementary carboxylic group –COOH group of salicylic acid (SAL) are optimal sites of ester bonds for synthesizing the prodrug DIT-SAL, comprising dithranol and salicylic acid in a 1:1 stoichiometric ratio (Figure 4).

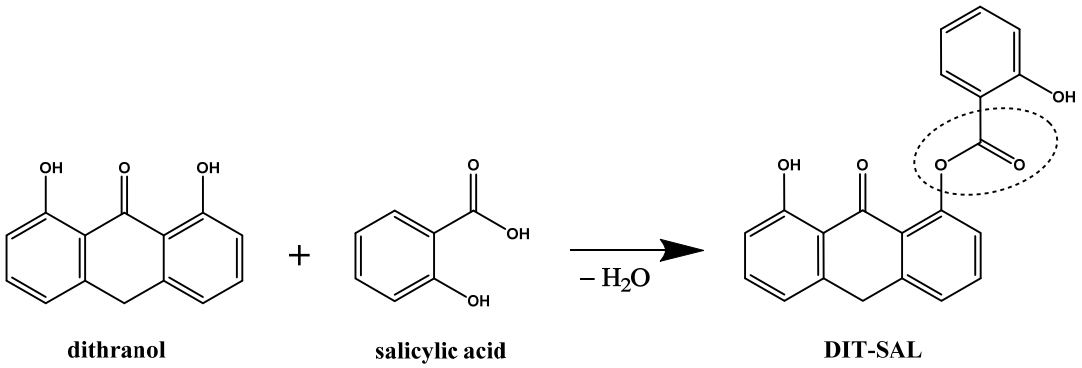

Figure 4. Proposed structure of a novel antipsoriatic prodrug DIT-SAL (8-hydroxy-9-oxo-9,10-dihydroanthracen-1-yl-2-hydroxybenzoate) formed by ester bond between dithranol and salicylic acid.

Such a conjugation of DIT and SAL can lead to better skin absorption than for original drugs, as has been demonstrated, e.g., for a naproxen–dithranol antipsoriatic prodrug [39,40], as well as for a hydroquinone–salicylic acid prodrug [41] for the treatment of melasma.

The aim of this work is to find the molecular structure, vibrational spectra, molecular orbitals, MEP (molecular electric potential), UV-VIS spectra, TDOS (total density of states), RDG (reduced density gradient) analysis, and ADME in silico modelling of the DIT-SAL molecule by using reliable computational methods of quantum chemistry.

2. Computational Methods

The calculations in this study were performed using the following theoretical methods or programs:

Density functional theory (DFT) is a quantum mechanical modelling method used to study the electronic structure of molecules and solids. It provides a way to calculate the properties of a system based on the electron density distribution.

Time-dependent DFT (TDDFT) extends DFT to study electronic excitations, such as those involved in optical and UV-VIS spectroscopy. It is particularly useful for the calculation of UV-VIS spectra, providing information about electronic transitions between molecular orbitals.

B3LYP Functional: Becke's three-parameter hybrid exchange functional [42], combined with the Lee–Yang–Parr gradient-corrected correlation, is a specific functional used in DFT calculations. B3LYP is known for its good performance in predicting a wide range of molecular properties.

The 6-311++G(d,p) basis set is a set of mathematical functions used to approximate the wavefunctions of electrons in a molecule. In this case, the 6-311++G(d,p) basis set is employed, which is relatively large and versatile.

The Gaussian 09 [43] program is a widely used computational chemistry software suite. In this study, this program was employed to perform the DFT and TDDFT calculations. The results were visualized using the GaussView 3 molecular visualization package [44].

Calculating vibrational frequencies helps confirm the stability of the molecular geometries. Imaginary frequencies indicate unstable structures. The absence of imaginary frequencies suggests that the computed geometries correspond to energy minima.

Multiwfn ver. 3.7 [45] is a program designed for analyzing wavefunction properties. In this study, the characteristics of the calculated wavefunction were studied with tools like the reduced density gradient (RDG) and total density of states (TDOS) methods.

The in silico modelling of the drug's pharmacokinetic profile, including toxicity (ADME), was performed using the SwissADME [46] and ADMETlab 2.0 [47] free online web platforms.

As has already been shown for many molecules [48–54], these theoretical methods are very reliable, giving theoretical results which are in harmony with experiments.

3. Results and Discussion

3.1. Molecular Structure of DIT-SAL

The optimized molecular geometry of DIT-SAL is displayed in Figure 5. The optimized bond lengths were determined using the DFT/B3LYP method with the 6-311++G(d,p) basis set. Naturally, for this new compound, there are no existing data on its structure. We have therefore been restricted to comparing it with dithranol and salicylic acid, which are structurally similar to the two parts of DIT-SAL joined by an ester bond and for which there are data available both from experiments [55] as well as from quantum chemistry computation [56–62] (Figures 6 and 7); for example, the calculated length of the two hydrogen bonds in dithranol is in very good agreement with the experimental value (1.69 Å versus experimental 1.60 Å). Also, the experimental length of the C=O bond (1.26 Å) is almost identical to the theoretical value (1.25 Å). Good agreement between theoretical and experimental values has also been obtained for salicylic acid, and it can therefore be expected that the theoretical values of the structural parameters for DIT-SAL are also reliable and would be useful for further research and the synthesis of this proposed antipsoriatic drug.

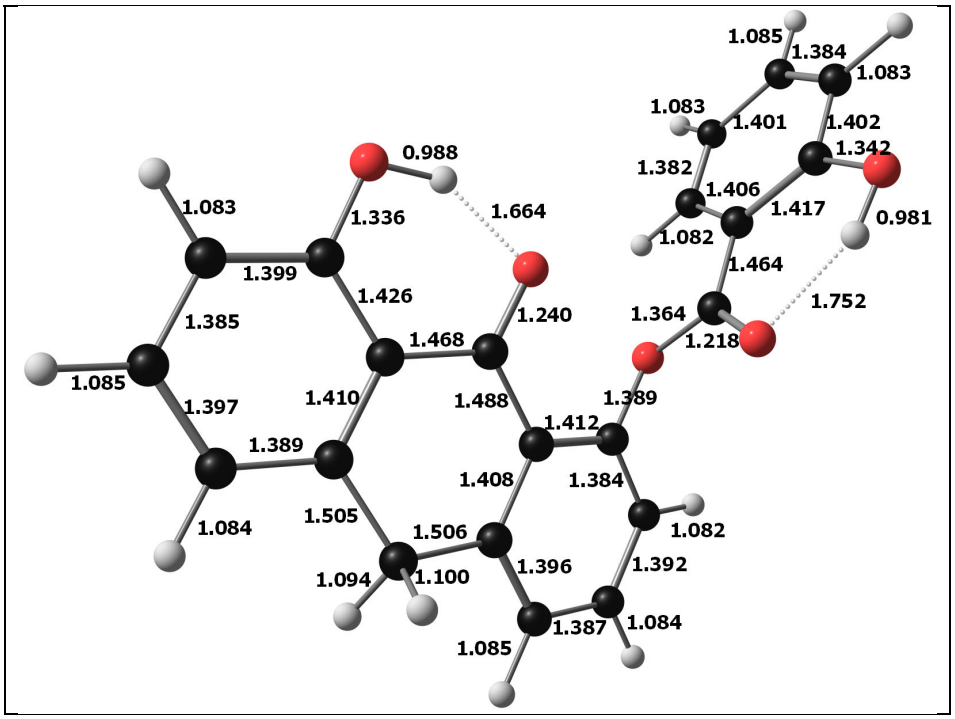

Figure 5. Molecular structure of DIT-SAL optimized with B3LYP/6-311++G(d,p).

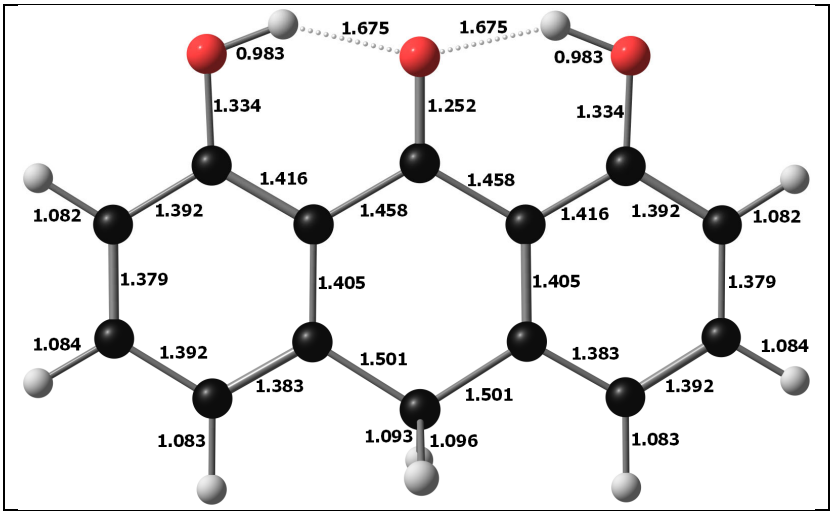

Figure 6. Molecular structure of dithranol optimized with B3LYP/6-311++G(d,p).

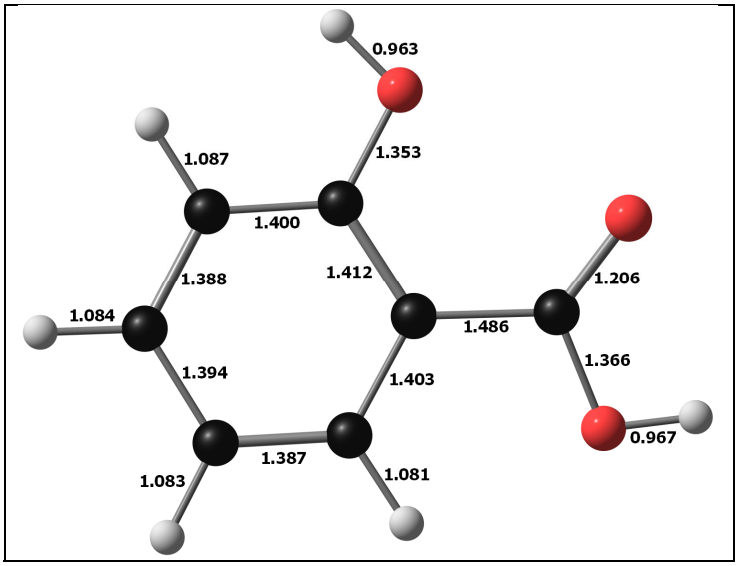

Figure 7. Molecular structure of salicylic acid optimized with B3LYP/6-311++G(d,p).

The values of some of the calculated properties of SAL-DIT's structure (dipole moment value, entropy, SCF energy, etc.) are shown in Table 1. The orientation of the dipole moment is shown in Figure 8.

Table 1. Properties of SAL-DIT's structure obtained using the DFT method.

Dipole Moment = (3.2541, 3.1276, −1.6948) 4.8211 D
Entropy = 148.643 cal/mol.K
Heat Capacity = 79.744 cal/mol.K
Molecular Mass = 346.08412
SCF Energy = −743680.78 kcal/mol
Thermodynamic Energy = 202.013 kcal/mol
Zero-Point Energy = 189.608733 kcal/mol

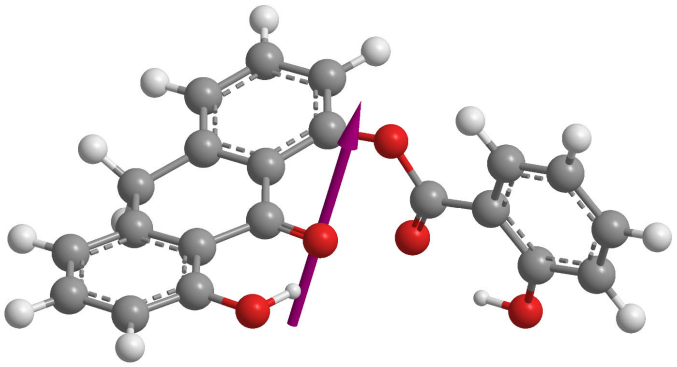

Figure 8. Orientation of total dipole moment of SAL-DIT's optimized structure.

All the proposed optimized geometries were confirmed to correspond to equilibrium structures through a vibrational analysis, without imaginary normal modes. These frequency calculations also provided us with the predicted IR vibrational spectra (Figure 9).

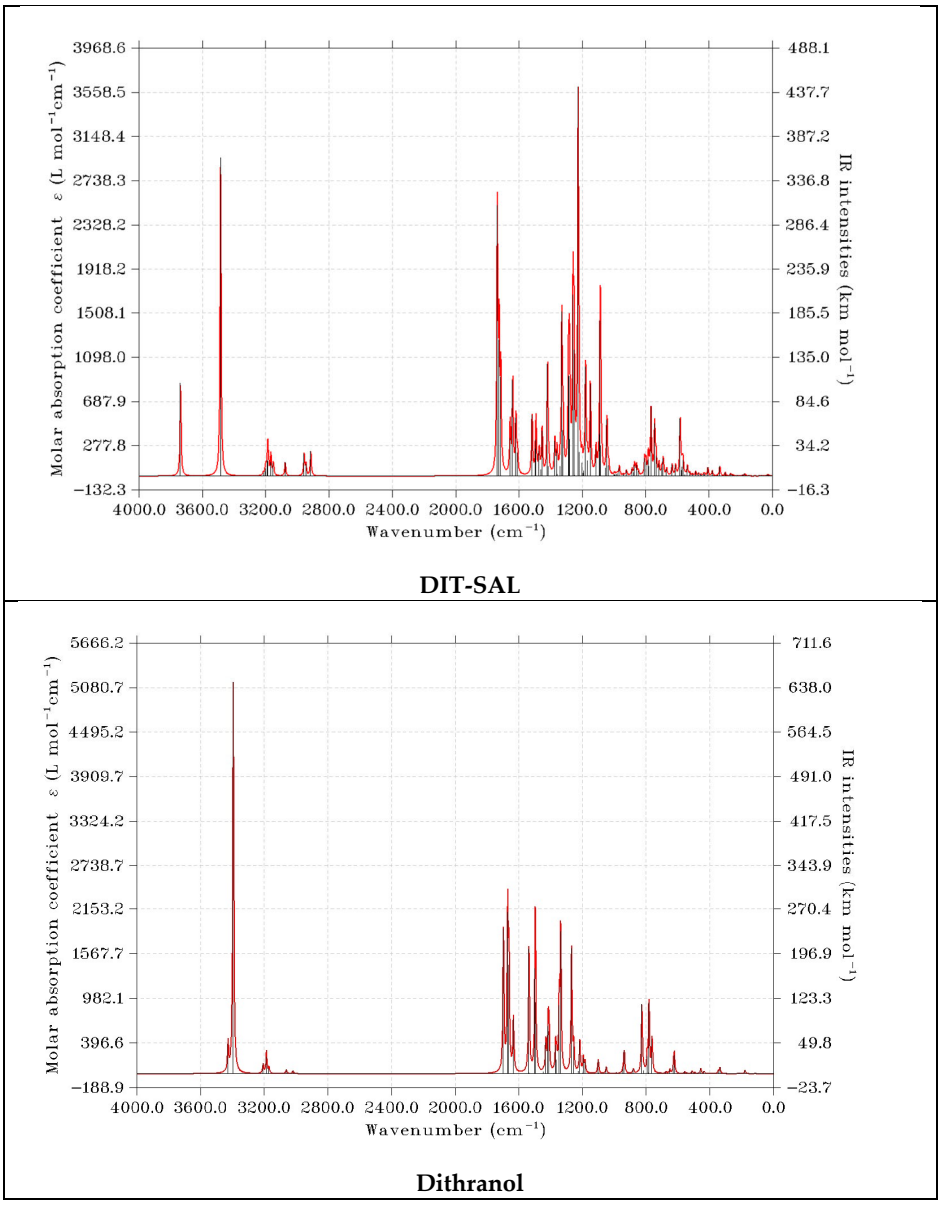

Figure 9. *Cont.*

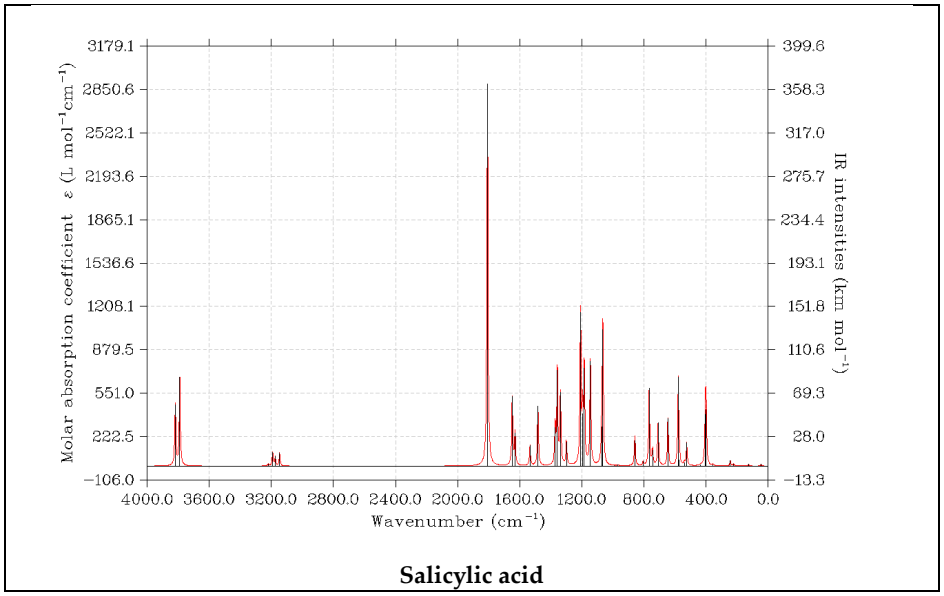

Figure 9. Comparison of infrared spectra of DIT-SAL, dithranol, salicylic acid, and molecules.

3.2. Frontier Molecular Orbitals

The quantum chemical calculation results in a set of molecular orbitals for the molecule under consideration. These orbitals represent the spatial distribution of electrons within the molecule. Frontier molecular orbitals (FMOs) are of particular interest from a chemical perspective because they play a crucial role in various chemical reactions and the properties of the molecules [63].

The HOMO (Highest Occupied Molecular Orbital) is the molecular orbital with the highest energy level that is occupied by electrons. It represents the outermost electrons in a molecule and is involved in electron donation during chemical reactions.

The LUMO (Lowest Unoccupied Molecular Orbital) is the molecular orbital with the lowest energy level that is unoccupied. It represents an area where electrons can be accepted during chemical reactions.

The HOMO and LUMO are often considered the most important molecular orbitals because they influence the reactivity and properties of a molecule. For example: The HOMO influences electron-donating abilities, nucleophilic reactions, and interactions with electron acceptors. The LUMO influences electron-accepting abilities, electrophilic reactions, and interactions with electron donors. Understanding the FMOs helps predict and interpret various chemical phenomena, such as reaction mechanisms, molecular stability, and electronic transitions.

In summary, the quantum chemical calculation of molecules provides information about their molecular orbitals. A decrease in the HOMO–LUMO energy gap (Equation (1)) signifies a possible charge transfer interaction taking place within a molecule because of the strong electron-accepting ability of the electron acceptor groups. Approximate ionization energy (*IE*) and electron affinity (*EA*) calculations (Equations (2) and (3)) based on these ideas are known as the so-called Koopmans theorem. The HOMO and LUMO energies are used to define the global chemical reactivity descriptors [64], where η denotes the global chemical hardness (Equation (4)), ζ denotes the global chemical softness (Equation (5)), and μ represents the electronic chemical potential (Equation (6)), which describes the charge transfer within a system in its ground state. Compounds with greater values of chemical potential are more reactive than those with small electronic chemical potentials. The global electrophilicity index, ω (Equation (7)), is a concept used in theoretical chemistry to assess the electrophilic character of a molecule or a chemical species. A higher electrophilicity index indicates a higher tendency of a system to accept electrons and, therefore, a higher

electrophilic character. This index is often used in the context of the Parr function [65], which is part of the conceptual density functional theory (CDFT).

$$E_g = E_{LUMO} - E_{HOMO} \quad (1)$$

$$EA = -E_{LUMO} \quad (2)$$

$$IP = -E_{HOMO} \quad (3)$$

$$\eta = \frac{IP - EA}{2} \quad (4)$$

$$\zeta = \frac{2}{IP - EA} \quad (5)$$

$$\mu = -\frac{IP + EA}{2} \quad (6)$$

$$\omega = \frac{\mu^2}{2\eta} \quad (7)$$

The HOMO and LUMO isosurface maps of DIT-SAL, and, for comparison, also two constituent molecules, are presented in Figures 10–12. As can be seen from Figure 10, the HOMO of DIT-SAL is distributed mostly on the salicylic acid part of the molecule, and on the other hand, the LUMO is localized mostly on the dithranol fragment of DIT-SAL. Interestingly, for HOMO-1, as well as for LUMO+1, this localization of the orbitals is exchanged. The first FMO delocalized across the whole DIT-SAL molecule is HOMO-2. The energy gap of DIT-SAL (Table 2) is 3.915 eV, almost the same as for dithranol (4.062 eV), indicating that the SAL-DIT molecule is chemically stable and may be considered a strong electrophile because its ω (4.772 eV) is substantially greater than 1.5 eV [66]. This finding is also supported by its rather high chemical hardness, which was found to be 1.958 eV. Its ionization potential value (6.280 eV) is higher than its electron affinity, which suggests the higher electron donor than lower electron acceptor capabilities (2.365 eV) of DIT-SAL.

Table 2. FMO energies and global chemical reactivity descriptors.

Molecule	Orbital	Energy (eV)	Energy Gap (E_g) (eV)	Electron Affinity (EA) (eV)	Ionization Potential (IP) (eV)	Chemical Hardness (η) (eV)	Chemical Softness (ζ) (eV^{-1})	Chemical Potential (μ) (eV)	Electrophile (ω) (eV)
SAL-DIT	E_{HOMO}	−6.280	3.915	2.365	6.280	1.958	0.511	−4.323	4.772
	E_{LUMO}	−2.365							
Dithranol	E_{HOMO}	−6.368	4.062	2.306	6.368	2.031	0.492	−4.337	4.631
	E_{LUMO}	−2.306							
Salicylic acid	E_{HOMO}	−6.576	5.153	1.423	6.576	2.568	0.389	−4.000	3.115
	E_{LUMO}	−1.423							

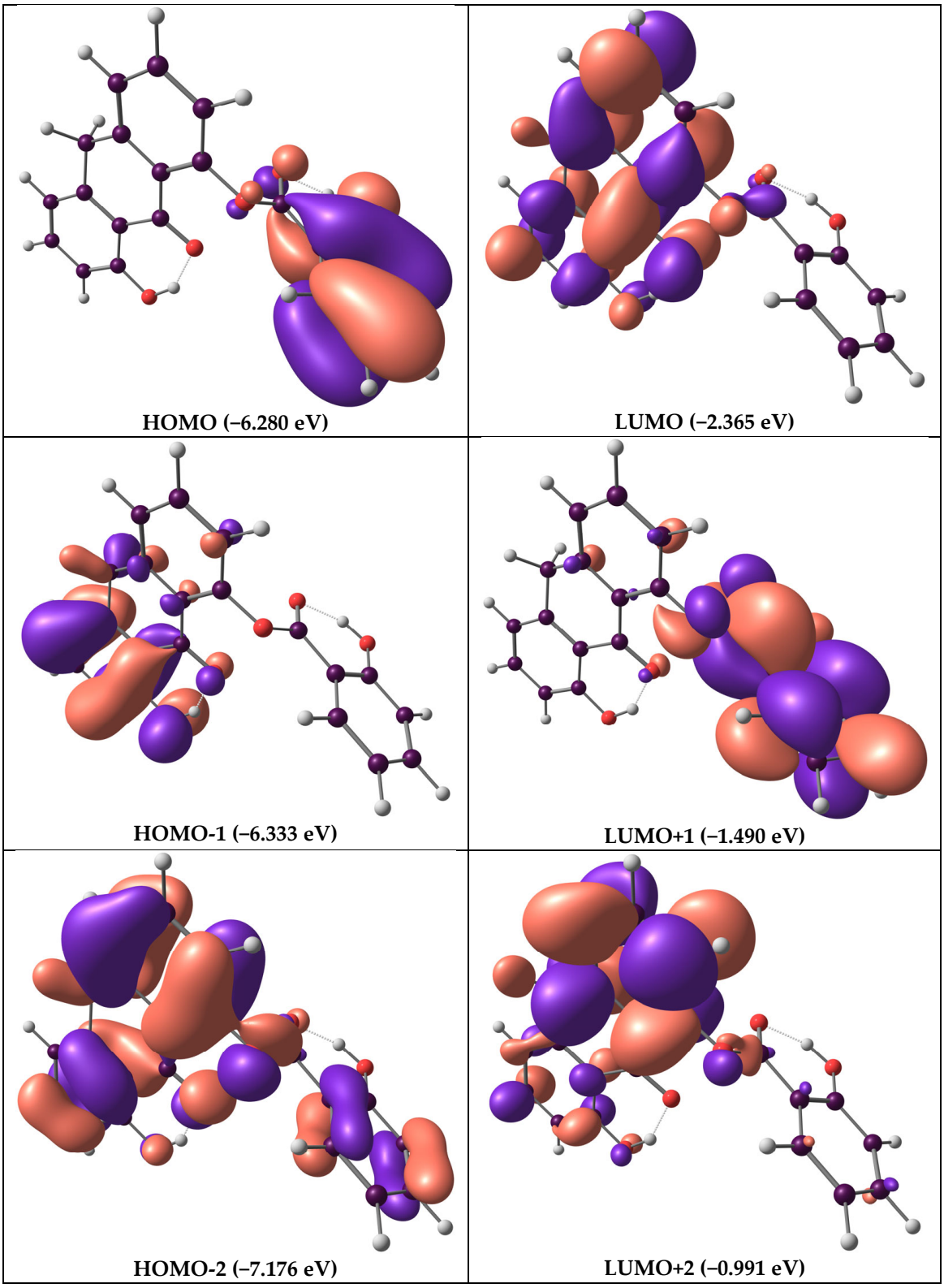

Figure 10. Shapes and energies of frontier molecular orbitals of DIT-SAL.

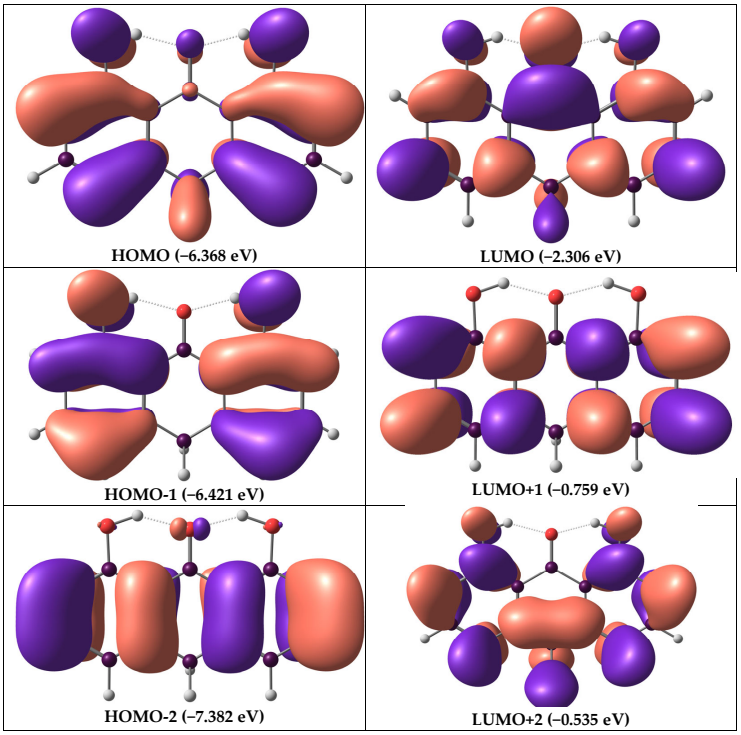

Figure 11. Shapes and energies of frontier molecular orbitals of dithranol.

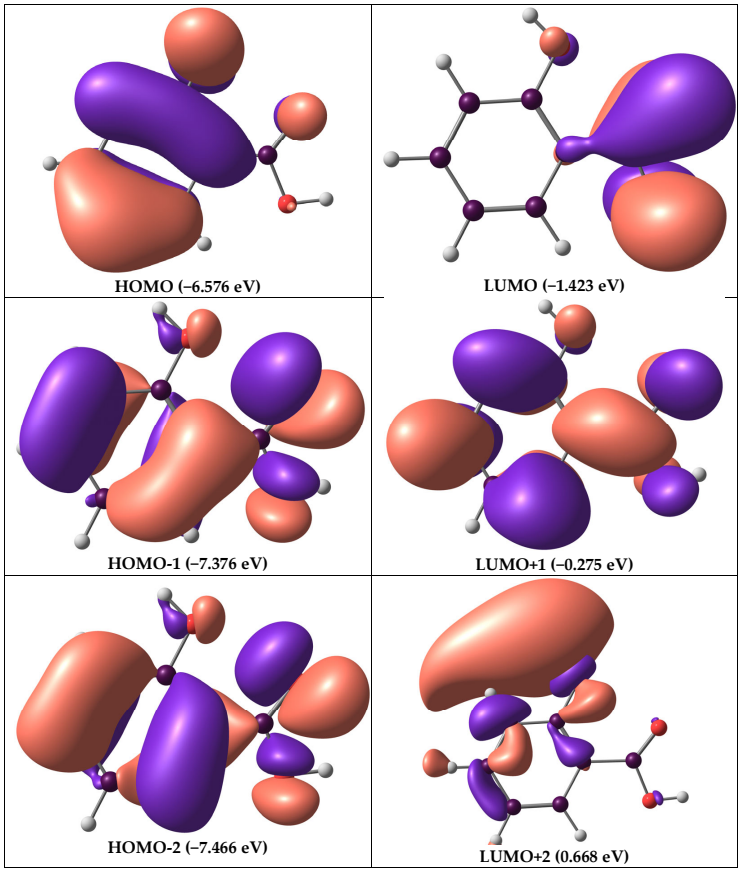

Figure 12. Shapes and energies of frontier molecular orbitals of salicylic acid.

3.3. TDOS (Total Density of States) Calculation

The TDOS was simulated by convoluting molecular orbitals with Gaussian curves. Convolution is a mathematical operation that combines two functions to produce a third one, often representing some property of interest. Gaussian functions are often used in computational chemistry and physics to represent distributions. In this context, it seems like Gaussian curves are being used to smooth or broaden the individual molecular orbitals. Gaussian curves with unit height typically mean that the area under each Gaussian curve is normalized to one. This is a common practice to ensure that the convolution operation does not alter the overall intensity or scale of the original molecular orbitals. Each discrete vertical line in the simulated spectrum likely corresponds to a specific molecular orbital. The position of these lines reflects the energy levels associated with each orbital. The dashed line highlights the position of the HOMO (Figure 13). This is a key parameter in understanding the electronic structure of the system [67]. The UV-VIS spectra for all the studied molecules are shown in Figure 14. For the calculations, we used the TDDFT method with the B3LYP/6-311++G(d,p) basis set. The most intensive peak in the DIT-SA UV-VIS spectrum corresponds to a transition from HOMO-1 to LUMO+1.

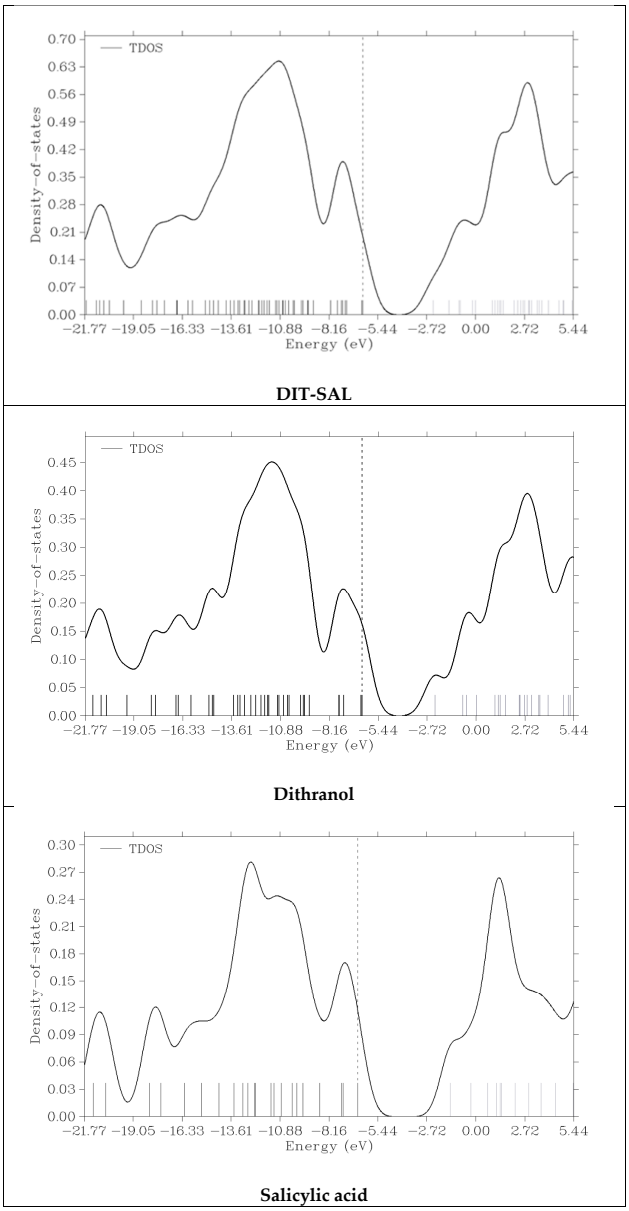

Figure 13. Total density of states (TDOS) for all studied molecules.

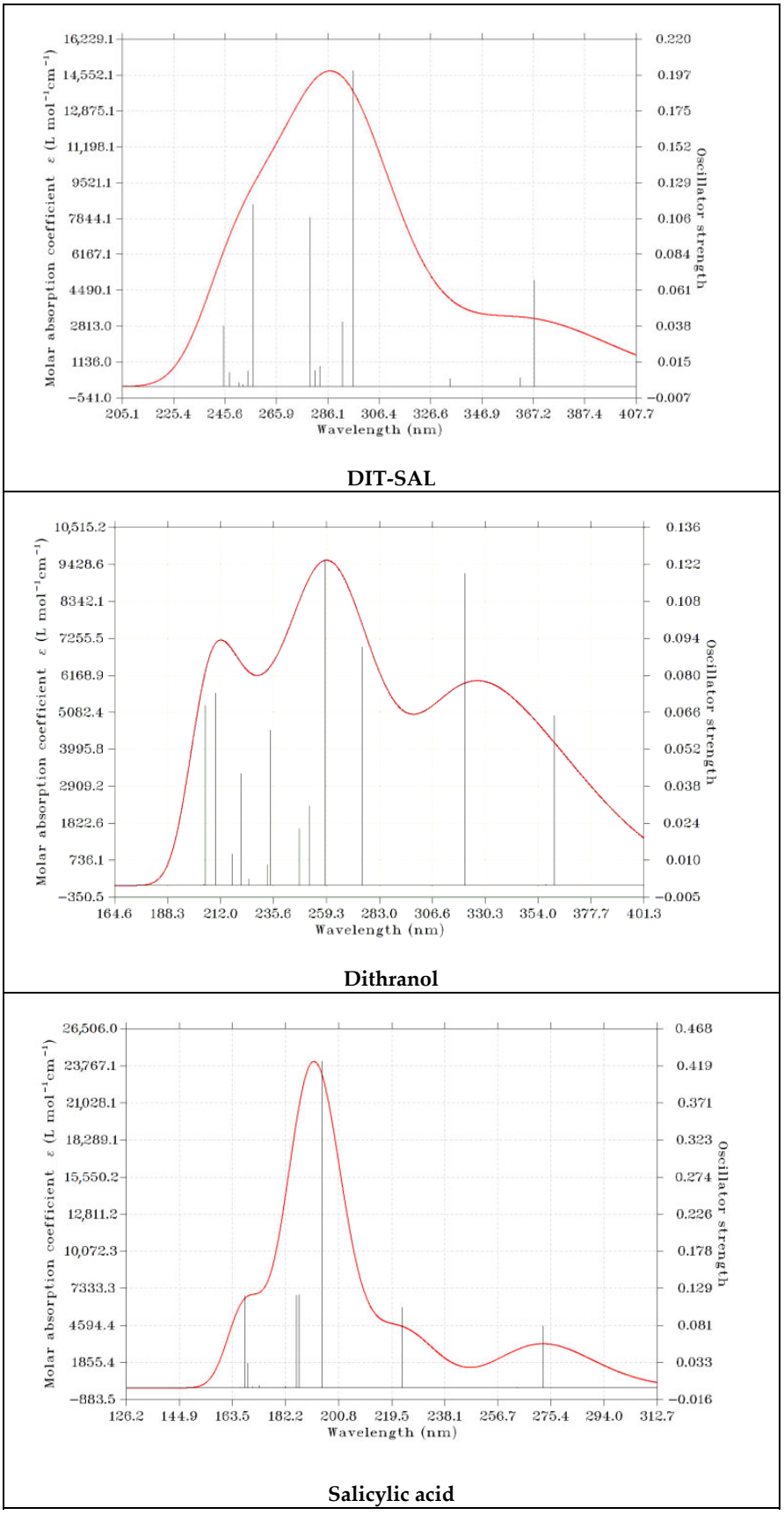

Figure 14. Comparison of UV-VIS spectra of dithranol, salicylic acid, and DIT-SAL calculated using the time-dependent DFT method.

3.4. The Molecular Electrostatic Potential (MEP)

The MEP can be calculated using the following formula [66]:

$$V(r) = \sum_A \left(\frac{Z_A}{|R_A - r|} - \int \frac{\rho(r)dr'}{r' - r} \right)$$

where Z_A denotes the charge of the nucleus A located in R_A and $\rho(r)$ is the density of electric charge. It displays probable regions for the electrophilic interaction of charged reagents with a given molecule [68,69]. The total electron density as well as the charge density of DIT-SAL are shown in Figure 15.

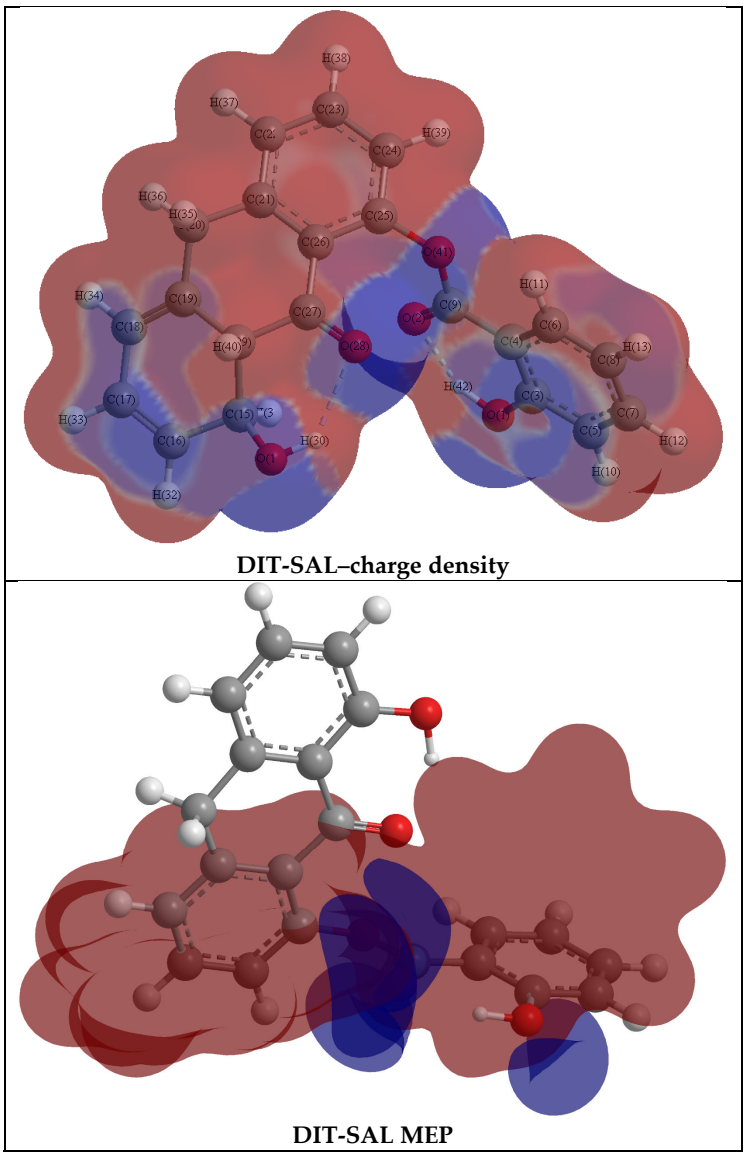

Figure 15. Distribution of total charge density and mean electrostatic potential (MEP) around DIT-SAL molecule. Positive and negative values are depicted in red and blue, respectively.

For the DIT-SAL molecule, the negative charges are mainly localized on the oxygen atoms, which have a higher electronegativity value and consequently have a higher electron density around them. The molecular electrostatic potential surface shows that the negative potential site is around the electronegative oxygen atoms and the positive potential sites are around the hydrogen and carbon atoms, as can also be seen from the distribution of charge. A pronounced area with negative values of potential and charge density is around the ester

bond, which may allow for the attack of polarized water ($OH^-...H^+$) on carbonyl oxygen, leading to esterase-catalyzed DIT-SAL hydrolysis. Carboxyl esterases, acetylcholinesterases, butyrylcholinesterases, paraoxonases, arylesterases, and biphenyl hydrolase-like protein (BPHL) are examples of enzymes that are responsible for the hydrolytic bioactivation of ester prodrugs.

3.5. Non-Covalent Interaction-Reduced Density Gradient (NCI-RDG)

We characterized the types of interactions occurring in the system using the non-covalent interaction-reduced density gradient (NCI-RDG) approach. The NCI method utilizes an RDG to visualize spatial interactions, where the RDG is a dimensionless quantity derived from the electron density and its first derivative. The method was developed by Johnson et al. [70], and the RDG is defined as follows:

$$RDG(r) = \frac{1}{2\sqrt[3]{3\pi^2}} \frac{|\nabla\rho(r)|}{\rho(r)^{\frac{4}{3}}} \quad (8)$$

The RDG was plotted against (sign λ_2)ρ to generate an NCI-RDG scattered diagram. The nature of the interaction can be predicted by the (sign λ_2)ρ values (where λ_2 is the second eigenvalue of the Hessian electronic density matrix) as follows:

1. (sign λ_2)$\rho > 0$: repulsive/steric effects;
2. (sign λ_2)$\rho < 0$: attractive interactions (hydrogen bonding);
3. (sign λ_2)$\rho \simeq 0$: van der Waals forces, which arise from overlapping electron clouds and occur over larger distances. The colored RDG scatter plots in Figure 16 were prepared using Multiwfn 3.7 software and plotted using Gnuplot version 5.4.

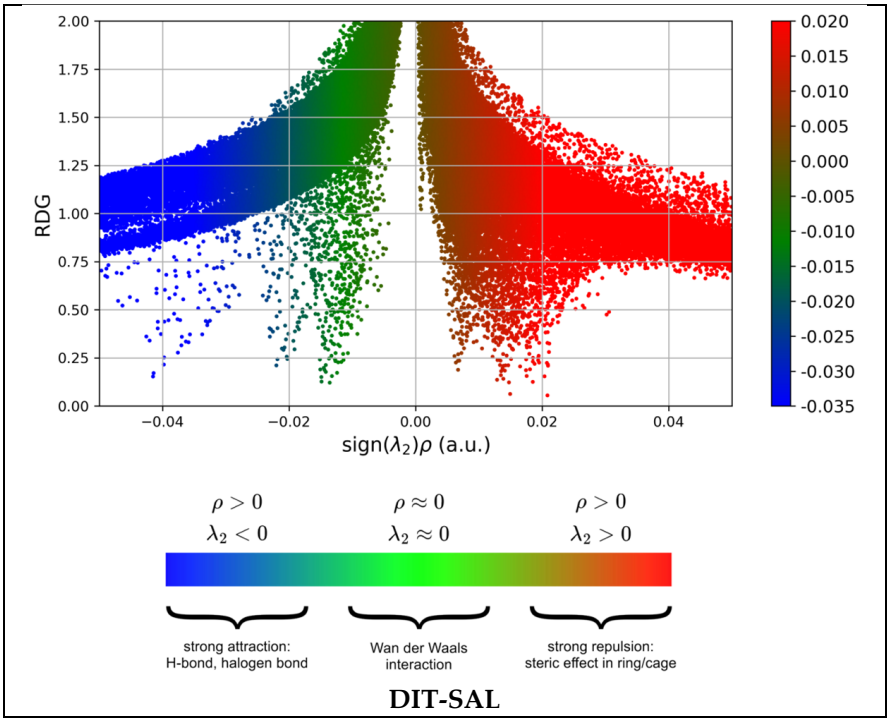

Figure 16. *Cont.*

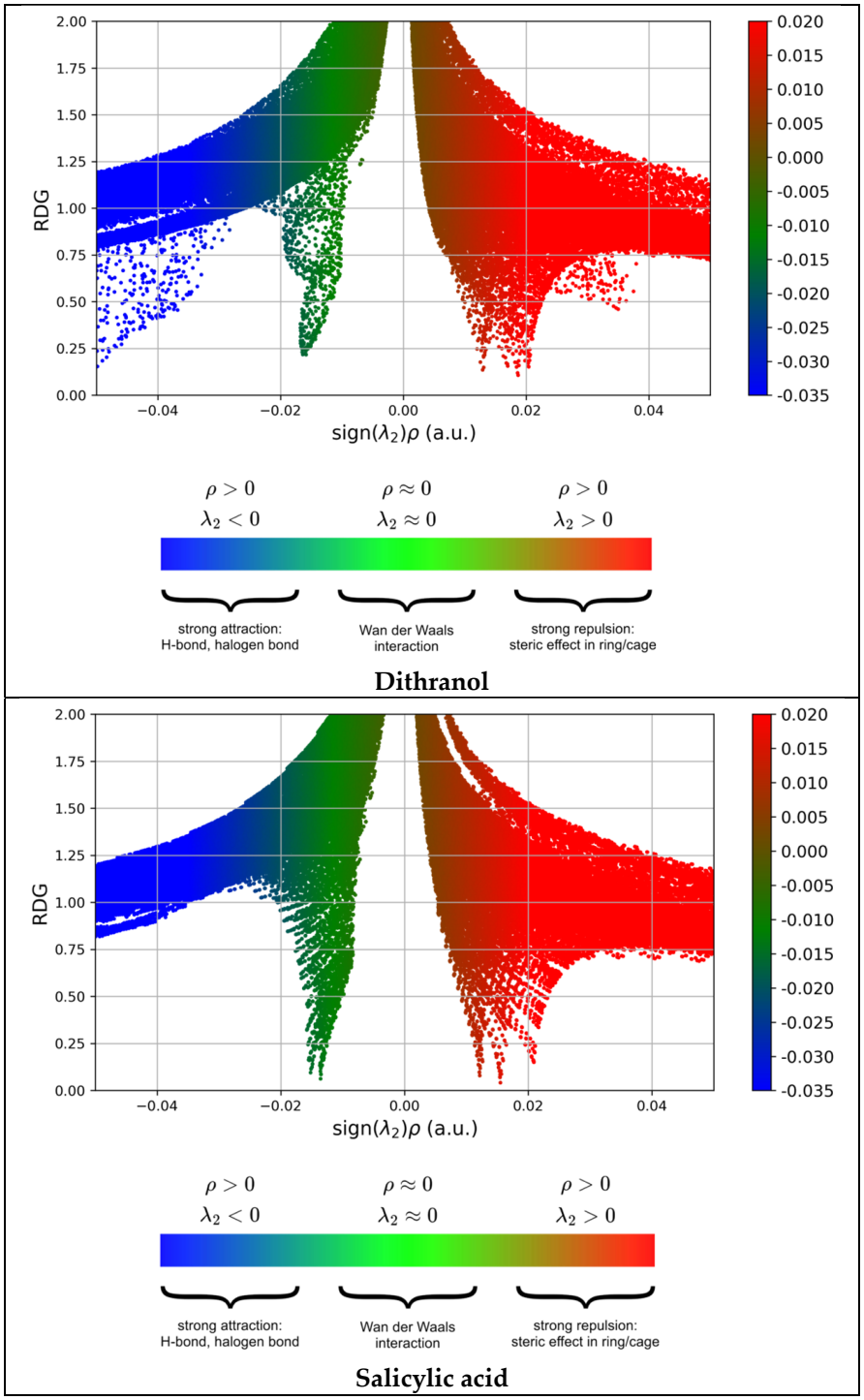

Figure 16. Scatter plot of RDG (reduced density gradient) for all studied molecules.

From Figure 16, the importance of two strong intra-molecular hydrogen bonds for both DIT-SAL and dithranol is clearly seen, which stabilize these molecules. What is interesting is that salicylic acid is not stabilized by hydrogen bonding (as can also be seen from the RDG plot), but when it is part of the DIT-SAL molecule, it participates in the formation of a form of hydrogen-bond-mediated stabilization of the proposed drug.

3.6. UV-VIS Spectra of DIT-SAL Degradation Products

We also found that the possible degradation products of DIT-SAL (in analogy with dithranol oxidation products [59], namely danthron-SAL (Figure 17)) have modified chro-

mophores with a molar absorption coefficient of 4863 L mol^{-1} c^{-1} at 417 nm, as compared with danthron's molar absorption coefficient of 8200 L mol^{-1} c^{-1} at 425 nm (Figure 18), which indicates that DIT-SAL's degradation products would have reduced staining properties, which would possibly be another beneficiary effect of DIT-SAL.

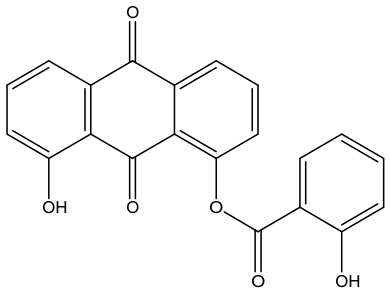

8-hydroxy-9,10-dioxo-9,10-dihydroanthracen-1-yl 2-hydroxybenzoate

Figure 17. Chemical structure of danthron–SAL.

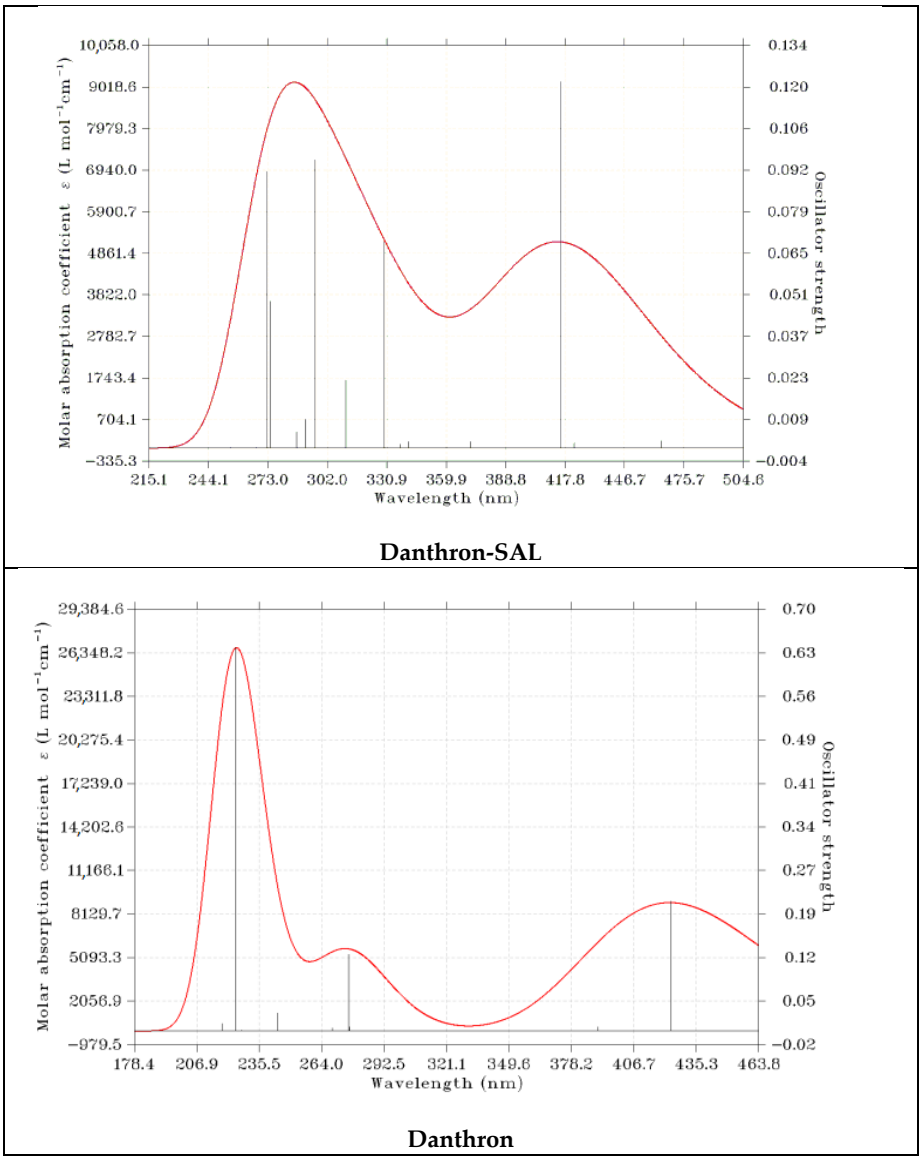

Figure 18. Comparison of UV-VIS spectra of danthron and danthron–SAL.

3.7. Structure of DIT-SAL in Dichloromethane

The polarized continuum model (PCM) is a theoretical approach used in computational chemistry to include the effects of a solvent in the calculation of molecular properties. It is particularly useful in studying the behavior of molecules in a solution. The PCM assumes that the solvent can be treated as a continuous medium with a defined dielectric constant, and it provides a way to incorporate the solvent environment into quantum mechanical calculations. In Figure 19, we have, as an illustration, the calculated structure of DIT-SAL in dichloromethane solvent. Comparing it with the in vacuo structure obtained at the same computational level shown in Figure 5, we can see only small changes in the bond length; nevertheless, in the future, it would be interesting to use the density functional developed for the study of weak molecular interactions [71].

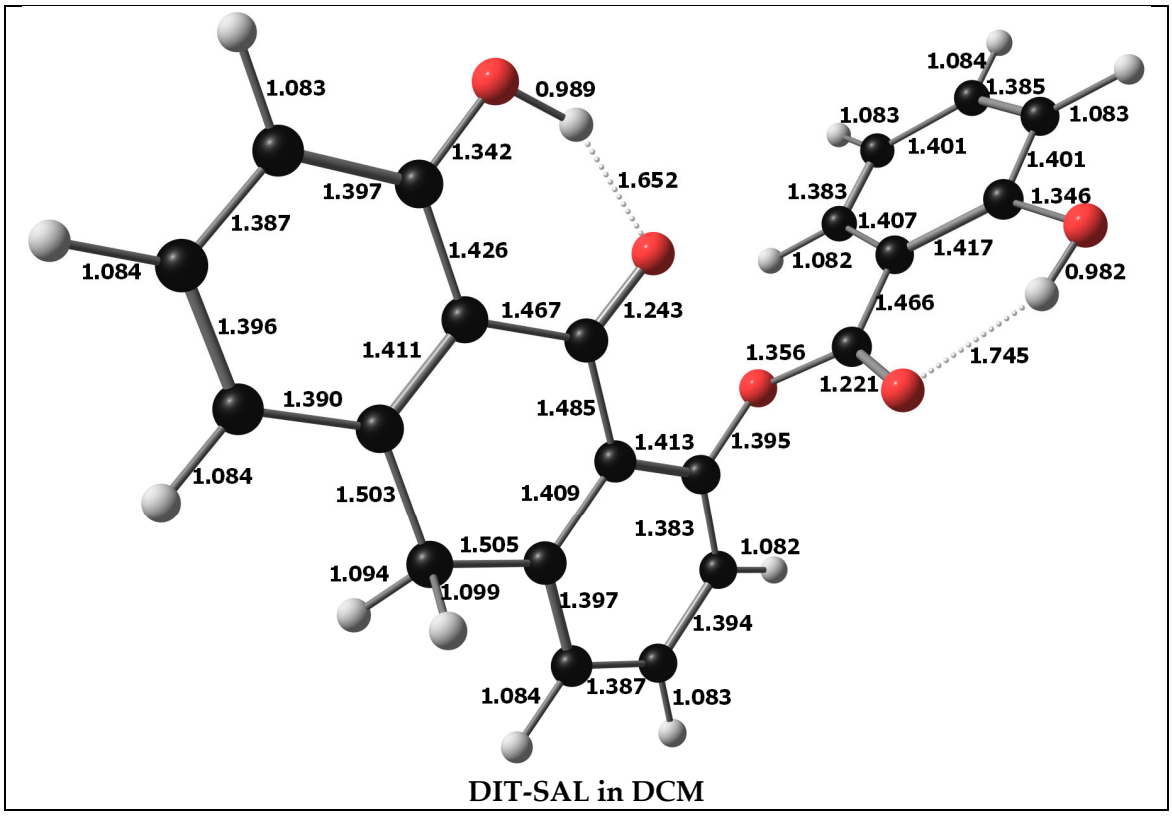

Figure 19. Molecular structure of DIT-SAL in dichloromethane optimized with B3LYP/6-311++G(d,p) using the PCM model.

3.8. ADME In Silico Modelling of DIT-SAL

ADME (absorption, distribution, metabolism, and excretion) properties play a crucial role in determining the pharmacokinetics and bioavailability of a drug, using, e.g., Lipinski's rule of five, which states a guideline to assess the drug-likeness of a compound based on its physicochemical properties [72]. The bioavailability radar obtained using SwissADME (Figure 20) is a picture of six physicochemical parameters, such as size, lipophilicity, polarity, solubility, saturation, and flexibility. The middle pink hexagon shows the optimal bioavailability zone for oral administration. Based on these calculations, the molecule of interest, SAL-DIT, has good qualities, as shown in Supplementary Table S1, similar to those of dithranol (Supplementary Table S2), obtained using ADMETLab 2.0.

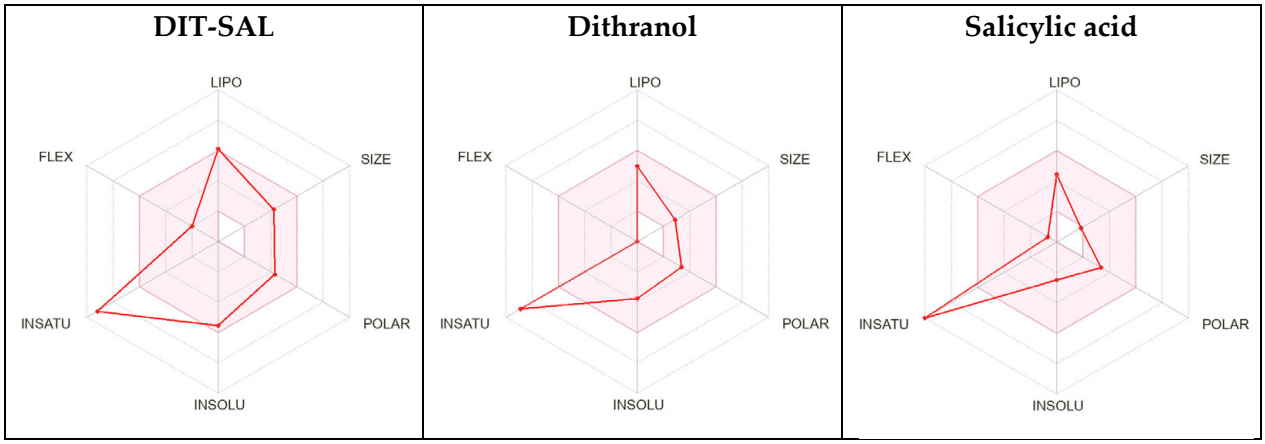

Figure 20. ADME radar structure (ideal values lie in pink area) for all three molecules studied (lipophilicity—LIPO; size as molecular weight—SIZE; polarity—POLAR (topological polar surface area); insolubility in water—INSOLU; insaturation—INSATU; flexibility as per rotatable bonds—FLEX).

For effective permeability, the optimal molecular weight is between 200 and 500 Da. The total molecular weight of the DIT-SAL molecule is 346 Da, which is in the range needed for optimal transport to the skin. The octanol–water partition coefficient (log P) found for DIT-SAL is 4.58, as compared with 3.56 for dithranol. The conjugates with higher log P values than the parent drugs indicate increased lipophilicity, while reduced aqueous solubility is observed. The hydroxyl moiety in dithranol and salicylic acid molecules plays a crucial role in aqueous solubility through hydrogen bonding. Esterification hinders this hydrogen bonding process. This interference in hydrogen bonding is likely responsible for the decreased solubility of prodrugs. Essentially, when esterification occurs, it disrupts the ability of the drug molecules to form hydrogen bonds with water molecules, leading to lower solubility in aqueous environments. This information can be valuable in understanding the physicochemical properties of drugs and their derivatives, which can impact factors like absorption and bioavailability in pharmaceutical applications. The lipophilic nature of the stratum corneum means that it has an affinity for lipid-soluble (lipophilic) substances. Permeants that are more lipophilic tend to partition more easily from the vehicle (the formulation applied to the skin) into the stratum corneum. This process is crucial for enhanced skin absorption because lipophilic substances can penetrate the lipids of the stratum corneum more readily. Once these lipophilic substances have penetrated the stratum corneum, they may further pass through into the underlying layers of the epidermis. This enhanced absorption can lead to the formation of a cutaneous reservoir within the whole skin, allowing for a sustained release of the substance over time. Hydrophilic substances may have difficulty penetrating the skin and may require specific formulation strategies to enhance their absorption.

3.9. Further Molecular Alternatives to DIT-SAL for Therapy of Psoriasis

There is also the possibility that two salicylic acid molecules could be conjugated to dithranol for the preparation of a diester prodrug in a 1:2 stoichiometric ratio (Figure 21).

Another interesting possibility would be to use acetylsalicylic acid (ASA, aspirin) instead of SAL for the construction of the dithranol–acetylsalicylic acid (DIT-ASA) prodrug (Figure 22).

Aspirin, or acetylsalicylic acid, is a medication commonly used for its analgesic, antipyretic, and anti-inflammatory properties. The ester bond in aspirin is formed between the acetyl group and the hydroxyl group of salicylic acid. The chemical reaction involves the acetylation of salicylic acid, resulting in the formation of aspirin and acetic acid (Figure 23). The reaction is as follows:

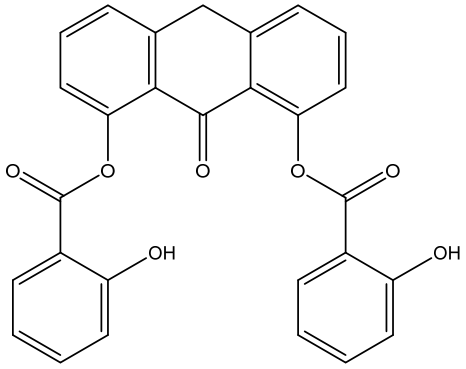

9-oxo-9,10-dihydroanthracene-1,8-diyl bis(2-hydroxybenzoate)

Figure 21. Structure of prodrug formed by two ester bonds between dithranol and two salicylic acid molecules.

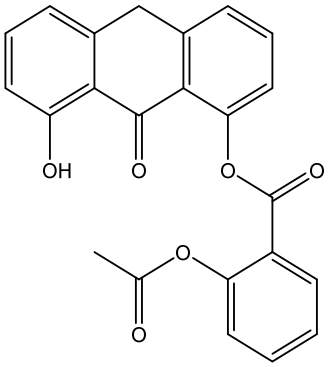

8-hydroxy-9-oxo-9,10-dihydroanthracen-1-yl-2-acetoxybenzoate

Figure 22. Chemical structure of prodrug formed by ester bond between dithranol and acetylsalicylic acid (aspirin) molecules.

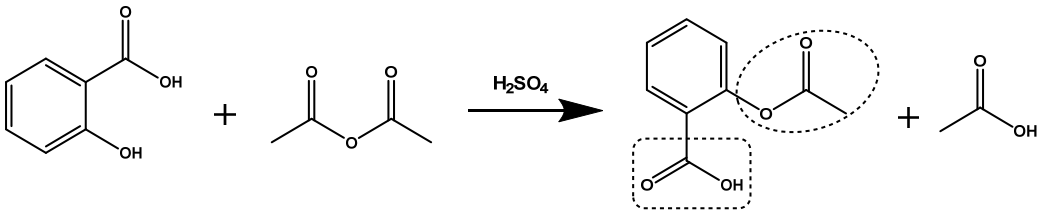

Figure 23. Reaction of salicylic acid with acetic anhydride leading to the synthesis of acetylsalicylic acid and the release of acetic acid. In dotted frames are shown ester bonds.

The specific ester bond in aspirin is between the oxygen atom of the hydroxyl group in salicylic acid and the carbon atom of the carbonyl group in acetic anhydride [73]. This ester linkage is what gives aspirin its chemical structure. The ester bond in aspirin is important for its pharmacological activity. Once ingested, aspirin is broken down in the body into salicylic acid, which exerts its therapeutic effects by inhibiting the action of enzymes involved in inflammation and pain (cyclooxygenases). The acetylation of salicylic acid improves the drug's properties and is one of the first examples of prodrug formation. It was introduced in 1897 when Felix Hoffmann modified the structure of salicylic acid and obtained acetylsalicylic acid, making it more stable and reducing its irritant effects on the gastrointestinal tract compared to salicylic acid alone [74]. We have two possibilities here: the first is the hydrolysis of the ester bond, directly producing dithranol and ASA, or a two-step process: first, the hydrolysis of ASA, giving us acetic acid and DIT-SAL, and then the hydrolysis of a second ester bond, which would produce DIT and SAL. Another option

would even be to join two molecules of ASA to DIT, as we considered for SAL molecules. All these possibilities are challenging tasks, both in terms of theory and experiment.

4. Conclusions

In the present work, both structural and electronic properties, harmonic vibrational frequencies, the MEP (molecular electric potential), UV-VIS spectra, the TDOS (total density of states), and a RDG (reduced density gradient) analysis were analyzed theoretically using the DFT/B3LYP/6–311++G(d,p) method for a newly proposed antipsoriatic prodrug comprising dithranol and salicylic acid (DIT-SAL) joined together with an ester bond (8-hydroxy-9-oxo-9,10-dihydroanthracen-1-yl-2-hydroxybenzoate), as well as for its constituents and degradation products. Generally, it can be said that experimental (where available) and theoretical spectroscopic data are in harmony, and it can therefore be expected that the theoretical values of the structural parameters for DIT-SAL are reliable and would be useful for understanding this proposed antipsoriatic drug. The ester bond is cleavable by endogenous esterase hydrolyzing this bond and releasing dithranol and salicylic acid in a 1:1 stoichiometric ratio directly into psoriatic plaques for a prolonged period of time. Furthermore, the DIT-SAL molecule was evaluated for drug-likeness by employing in silico ADME experiments, further supporting DIT-SAL's usefulness. From the computed UV-Vis spectra, it is very probable that DIT-SAL's degradation products would have reduced staining properties, which would be another beneficiary effect of DIT-SAL. Our computational study may therefore be useful for the understanding of its properties, which may assist in the synthesis and further experimental study of this proposed antipsoriatic dual-action prodrug with reduced adverse effects and enhanced therapeutic efficacy.

Supplementary Materials: The following supporting information can be downloaded at https://www.mdpi.com/article/10.3390/app14031094/s1: Table S1: ADMET results for SAL-DIT; Table S2: ADMET results for dithranol.

Author Contributions: Conceptualization, validation, formal analysis, methodology, investigation, and data curation N.A., J.M., P.B., M.B. and M.Š.; writing—original draft preparation, N.A. and J.M.; writing—review and editing, M.B., J.M., P.B. and M.Š. All authors have read and agreed to the published version of the manuscript.

Funding: This research was funded by the Slovak Grant Agency VEGA project No. 1/0639/22.

Institutional Review Board Statement: Not applicable.

Informed Consent Statement: Not applicable.

Data Availability Statement: Data are contained within the article.

Conflicts of Interest: The authors declare no conflicts of interest.

References

1. Kocaaga, A.; Kocaaga, M. Psoriasis: An Immunogenetic Perspective. *Glob. Med. Genet.* **2022**, *9*, 82–89. [CrossRef]
2. Šimaljaková, M.; Buchvald, D. *Dermatovenereology*; Comenius University Press: Bratislava, Slovakia, 2019.
3. Griffiths, C.E.M.; Armstrong, A.W.; Gudjonsson, J.E.; Barker, J.N.W.N. Psoriasis. *Lancet* **2021**, *397*, 1301–1315. [CrossRef] [PubMed]
4. Armstrong, A.W.; Read, C. Pathophysiology, Clinical Presentation, and Treatment of Psoriasis: A Review. *JAMA* **2020**, *323*, 1945–1960. [CrossRef] [PubMed]
5. Šimaljaková, M. Psoriasis—Etiopathogenesis, clinical picture and current therapy options. *Dermatol. Prax* **2008**, *2*, 50–55.
6. Ali, Z.; Robert Zibert, J.; Dahiya, P.; Bachdal Johansen, C.B.; Grønlund Holm, J.; Ravn Jørgensen, A.H.; Manole, J.; Suru, A.; Egeberg, A.; Francis Thomsen, S.; et al. Mild-to-moderate severity of psoriasis may be assessed remotely based on photographs and self-reported extent of skin involvement. *JAAD Int.* **2023**, *11*, 129–136. [CrossRef] [PubMed]
7. Boehncke, W.H.; Schön, M.P. Psoriasis. *Lancet* **2015**, *386*, 983–994. [CrossRef] [PubMed]
8. Guo, L.; Jin, H. Research progress of metabolomics in psoriasis. *Chin. Med. J.* **2023**, *136*, 1805–1816. [CrossRef] [PubMed]
9. Ahmad, M.Z.; Mohammed, A.A.; Algahtani, M.S.; Mishra, A.; Ahmad, J. Nanoscale Topical Pharmacotherapy in Management of Psoriasis: Contemporary Research and Scope. *J. Funct. Biomater.* **2022**, *14*, 19. [CrossRef]

10. Babincová, N.; Jirsák, O.; Babincová, M.; Babinec, P.; Šimaljaková, M. Remote magnetically controlled drug release from electrospun composite nanofibers: Design of a smart platform for therapy of psoriasis. *Z. Naturforsch.* **2020**, *75*, 587–591. [CrossRef]
11. Andrýsková, N.; Sourivong, P.; Babincová, M.; Šimaljaková, M. Controlled Release of Tazarotene from Magnetically Responsive Nanofiber Patch: Towards More Efficient Topical Therapy of Psoriasis. *Appl. Sci.* **2021**, *11*, 11022. [CrossRef]
12. Sehgal, V.N.; Verma, P.; Khurana, A. Anthralin/dithranol in dermatology. *Int. J. Dermatol.* **2014**, *53*, 449–460. [CrossRef]
13. Ashton, R.E.; Andre, P.; Lowe, N.J.; Whitefield, M. Anthralin: Historical and current perspectives. *J. Am. Acad. Dermatol.* **1983**, *9*, 173–192. [CrossRef]
14. Seville, R.H. Advances in the use of anthralin. *J. Am. Acad. Dermatol.* **1981**, *5*, 319–321. [CrossRef]
15. Kadian, V.; Kumar, S.; Saini, K.; Kakkar, V.; Rao, R. Dithranol: An Insight into its Novel Delivery Cargos for Psoriasis Management. *Curr. Drug. Res. Rev.* **2020**, *12*, 82–96. [CrossRef] [PubMed]
16. Andrýsková, N.; Sourivong, P.; Babincová, M.; Babinec, P.; Šimaljaková, M. Electrospun PCL/PVA Coaxial Nanofibers with Embedded Titanium Dioxide and Magnetic Nanoparticles for Stabilization and Controlled Release of Dithranol for Therapy of Psoriasis. *Magnetochemistry* **2023**, *9*, 187. [CrossRef]
17. de Mare, S.; Calis, N.; den Hartog, G.; van Erp, P.E.; van de Kerkhof, P.C. The relevance of salicylic acid in the treatment of plaque psoriasis with dithranol creams. *Skin Pharmacol.* **1988**, *1*, 259–264. [CrossRef] [PubMed]
18. van de Kerkhof, P.C.; van der Valk, P.G.; Swinkels, O.Q.; Kucharekova, M.; de Rie, M.A.; de Vries, H.J.; Damstra, R.; Oranje, A.P.; de Waard-van der Spek, F.B.; van Neer, P.; et al. A comparison of twice-daily calcipotriol ointment with once-daily short-contact dithranol cream therapy: A randomized controlled trial of supervised treatment of psoriasis vulgaris in a day-care setting. *Br. J. Dermatol.* **2006**, *155*, 800–807. [CrossRef] [PubMed]
19. Unna, P.G. Cignolin als Heilmittel der Psoriasis. *Dermatol. Wochenschr.* **1916**, *7*, 150–163.
20. Benezeder, T.; Gehad, A.; Patra, V.; Clark, R.; Wolf, P. Induction of IL-1β and antimicrobial peptides as a potential mechanism for topical dithranol. *Exp. Dermatol.* **2021**, *30*, 841–846. [CrossRef] [PubMed]
21. Behrangi, E.; Roohaninasab, M.; Sadeghzadeh-Bazargan, A.; Najar Nobari, N.; Ghassemi, M.; Seirafianpour, F.; Goodarzi, A.; Dodangeh, M. A systematic review on the treatment of pediatric severe alopecia areata by topical immunotherapy or anthralin (contact sensitization) or low-level light/laser therapy (LLLT): Focus on efficacy, safety, treatment duration, recurrence, and follow-up based on clinical studies. *J. Cosmet. Dermatol.* **2022**, *21*, 2727–2741. [CrossRef] [PubMed]
22. Hindson, C.; Diffey, B.; Lawlor, F.; Downey, A. Dithranol-UV-A phototherapy (DUVA) for psoriasis: A treatment without dressings. *Br. J. Dermatol.* **1983**, *108*, 457–460. [CrossRef] [PubMed]
23. Kussini, J.; Charalambous, A.; Sachsenweger, F.; Steinert, M. Successful removal of anthralin staining from facial skin. *Int. J. Dermatol.* **2023**, *62*, 21–22. [CrossRef] [PubMed]
24. Thoma, K.; Holzmann, C. Photostability of dithranol. *Eur. J. Pharm. Biopharm.* **1998**, *46*, 201–208. [CrossRef]
25. Savian, A.L.; Rodrigues, D.; Weber, J.; Ribeiro, R.F.; Motta, M.H.; Schaffazick, S.R.; Adams, A.I.; de Andrade, D.F.; Beck, R.C.; da Silva, C.B. Dithranol-loaded lipid-core nanocapsules improve the photostability and reduce the in vitro irritation potential of this drug. *Mater. Sci. Eng. C Mater. Biol. Appl.* **2015**, *46*, 69–76. [CrossRef]
26. Melo, T.S.; Dubertret, L.; Prognon, P.; Gond, A.; Mahuzier, G.; Santus, R. Physicochemical properties and stability of anthralin in model systems and human skin. *J. Investig. Dermatol.* **1983**, *80*, 1–6. [CrossRef] [PubMed]
27. Mahrle, G.; Bonnekoh, B.; Ghyczy, M.; Wiegrebe, W. Stability of anthralin in liposomal phospholipids. *Arch. Dermatol. Res.* **1991**, *283*, 483–484. [CrossRef]
28. Herman, J.; Remon, J.P.; De Bersagues, J. Influence of storage conditions on the stability of anthralin in the presence of coal tar and salicylic acid in a white soft paraffin base. *J. Am. Acad. Dermatol.* **1988**, *18*, 750–751. [CrossRef]
29. Kruszewski, F.H.; DiGiovanni, J. Alterations in epidermal polyamine levels and DNA synthesis following topical treatment with chrysarobin in SENCAR mice. *Cancer Res.* **1988**, *48*, 6390–6395.
30. Müller, K. Antipsoriatic anthrones: Aspects of oxygen radical formation, challenges and prospects. *Gen. Pharmacol.* **1996**, *27*, 1325–1335. [CrossRef]
31. Müller, K.; Gawlik, I. Novel 10-substituted antipsoriatic anthrones as inhibitors of epidermal 12-lipoxygenase and lipid peroxidation in membranes. *Biochem. Pharmacol.* **1995**, *50*, 2077–2083. [CrossRef]
32. Müller, K.; Gürster, D.; Piwek, S.; Wiegrebe, W. Antipsoriatic anthrones with modulated redox properties. 1. Novel 10-substituted 1,8-dihydroxy-9(10H)-anthracenones as inhibitors of 5-lipoxygenase. *J. Med. Chem.* **1993**, *36*, 4099–4107. [CrossRef]
33. Müller, K.; Leukel, P.; Ziereis, K.; Gawlik, I. Antipsoriatic anthrones with modulated redox properties. 2. Novel derivatives of chrysarobin and isochrysarobin--antiproliferative activity and 5-lipoxygenase inhibition. *J. Med. Chem.* **1994**, *37*, 1660–1669. [CrossRef]
34. Prinz, H.; Wiegrebe, W.; Müller, K. Syntheses of Anthracenones. 3. Revised Preparative Route to 10-Benzoyl-1,8-dihydroxy-9(10H)-anthracenones. *J. Org. Chem.* **1996**, *61*, 2861–2864. [CrossRef]
35. Müller, K.; Reindl, H. Cornified envelope formation by anthralin, simple analogues, and related anthracenones. *Arch. Pharm.* **2001**, *334*, 86–92. [CrossRef]
36. Arif, T. Salicylic acid as a peeling agent: A comprehensive review. *Clin. Cosmet. Investig. Dermatol.* **2015**, *8*, 455–461. [CrossRef] [PubMed]
37. Lavis, L.D. Ester bonds in prodrugs. *ACS. Chem. Biol.* **2008**, *3*, 203–206. [CrossRef] [PubMed]

38. Liederer, B.M.; Borchardt, R.T. Enzymes involved in the bioconversion of ester-based prodrugs. *J. Pharm. Sci.* **2006**, *95*, 1177–1195. [CrossRef]
39. Lau, W.M.; White, A.W.; Heard, C.M. Topical delivery of a naproxen-dithranol co-drug: In vitro skin penetration, permeation, and staining. *Pharm. Res.* **2010**, *27*, 2734–2742. [CrossRef] [PubMed]
40. Lau, W.M.; Heard, C.M.; White, A.W. Design, synthesis and in vitro degradation of a novel co-drug for the treatment of psoriasis. *Pharmaceutics* **2013**, *5*, 232–245. [CrossRef]
41. Hsieh, P.W.; Aljuffali, I.A.; Fang, C.L.; Chang, S.H.; Fang, J.Y. Hydroquinone-salicylic acid conjugates as novel anti-melasma actives show superior skin targeting compared to the parent drugs. *J. Dermatol. Sci.* **2014**, *76*, 120–131. [CrossRef]
42. Becke, A.D. Density-functional thermochemistry. III. The role of exact exchange. *J. Chem. Phys.* **1993**, *98*, 5648–5652. [CrossRef]
43. Frisch, M.J.; Trucks, G.W.; Schlegel, H.B.; Scuseria, G.E.; Robb, M.A.; Cheeseman, J.R.; Scalmani, G.; Barone, V.; Mennucci, B.; Petersson, G.A. *Gaussian 09*, Revision, D.01; Gaussian, Inc.: Wallingford, CT, USA, 2013.
44. Frisch, A.E.; Keith, T.A.; Dennington, R.D. *GaussView Reference*; Semichem, Inc.: Irvine, CA, USA, 2003.
45. Lu, T.; Chen, F. Multiwfn: A multifunctional wavefunction analyzer. *J. Comput. Chem.* **2012**, *33*, 580–592. [CrossRef] [PubMed]
46. Daina, A.; Michielin, O.; Zoete, V. SwissADME: A free web tool to evaluate pharmacokinetics, drug-likeness and medicinal chemistry friendliness of small molecules. *Sci. Rep.* **2017**, *7*, 42717. [CrossRef] [PubMed]
47. Xiong, G.; Wu, Z.; Yi, J.; Fu, L.; Yang, Z.; Hsieh, C.; Yin, M.; Zeng, X.; Wu, C.; Lu, A.; et al. ADMETlab 2.0: An Integrated Online Platform for Accurate and Comprehensive Predictions of ADMET Properties. *Nucleic Acids Res.* **2021**, *49*, W5–W14. [CrossRef] [PubMed]
48. Rubab, S.L.; Raza, A.R.; Nisar, B.; Ashfaq, M.; Altaf, Y.; Hussain, R.; Sajjad, N.; Akram, M.S.; Tahir, M.N.; Shaheen, M.A.; et al. Synthesis, Crystal Structure, DFT Calculations, Hirshfeld Surface Analysis and In Silico Drug-Target Profiling of (R)-2-(2-(1,3-Dioxoisoindolin-2-yl)propanamido)benzoic Acid Methyl Ester. *Molecules* **2023**, *28*, 4375. [CrossRef] [PubMed]
49. Assad, M.; Paracha, R.N.; Siddique, A.B.; Shaheen, M.A.; Ahmad, N.; Mustaqeem, M.; Kanwal, F.; Mustafa, M.Z.U.; Rehman, M.F.U.; Fatima, S.; et al. In Silico and In Vitro Studies of 4-Hydroxycoumarin-Based Heterocyclic Enamines as Potential Anti-Tumor Agents. *Molecules* **2023**, *28*, 5828. [CrossRef] [PubMed]
50. Akman, F.; Demirpolat, A.; Kazachenko, A.S.; Kazachenko, A.S.; Issaoui, N.; Al-Dossary, O. Molecular Structure, Electronic Properties, Reactivity (ELF, LOL, and Fukui), and NCI-RDG Studies of the Binary Mixture of Water and Essential Oil of Phlomis bruguieri. *Molecules* **2023**, *28*, 2684. [CrossRef] [PubMed]
51. Kazachenko, A.S.; Tanış, E.; Akman, F.; Medimagh, M.; Issaoui, N.; Al-Dossary, O.; Bousiakou, L.G.; Kazachenko, A.S.; Zimonin, D.; Skripnikov, A.M. A Comprehensive Study of N-Butyl-1H-Benzimidazole. *Molecules* **2022**, *27*, 7864. [CrossRef] [PubMed]
52. Akman, F. Spectroscopic investigation, HOMO–LUMO energies, natural bond orbital (NBO) analysis and thermodynamic properties of two-armed macroinitiator containing coumarin with DFT quantum chemical calculations. *Can. J. Phys.* **2016**, *94*, 583–593. [CrossRef]
53. Abraham, C.S.; Prasana, J.C.; Muthu, S. Quantum mechanical, spectroscopic and docking studies of 2-Amino-3-bromo-5-nitropyridine by Density Functional Method. *Spectrochim. Acta A Mol. Biomol. Spectrosc.* **2017**, *181*, 153–163. [CrossRef]
54. Arulaabaranam, K.; Muthu, S.; Mani, G.; Ben Geoffrey, A.S. Speculative assessment, molecular composition, PDOS, topology exploration (ELF, LOL, RDG), ligand-protein interactions, on 5-bromo-3-nitropyridine-2-carbonitrile. *Heliyon* **2021**, *7*, e07061. [CrossRef]
55. Ahmed, F.R. The correct structural formula for anthralin. *Acta Crystallogr. B* **1980**, *36*, 3184–3186. [CrossRef]
56. Andersen, K.B.; Spanget-Larsen, J. Electronic transitions and intramolecular hydrogen bonding in anthralin. UV_VIS linear dichroism spectroscopy and quantum chemical calculations. *Spectrochim. Acta* **1997**, *53*, 2615–2625. [CrossRef]
57. Holder, A.J.; Upadrashta, S.M. A semiempirical computational investigation of the antipsoriatic drug anthralin. *J. Pharm. Sci.* **1992**, *81*, 1074–1078. [CrossRef] [PubMed]
58. Ellis, E.S.; MacHale, L.T.; Szilagyi, R.K.; DuBois, J.L. How Chemical Environment Activates Anthralin and Molecular Oxygen for Direct Reaction. *J. Org. Chem.* **2020**, *85*, 1315–1321. [CrossRef] [PubMed]
59. Czerwinska, M.; Sikora, A.; Szajerski, P.; Zielonka, J.; Adamus, J.; Marcinek, A.; Piech, K.; Bednarek, P.; Bally, T. Anthralin: Primary products of its redox reactions. *J. Org. Chem.* **2006**, *71*, 5312–5319. [CrossRef] [PubMed]
60. Maheshwary, S.; Lourderaj, U.; Sathyamurthy, N. Ab initio quantum chemical investigation of the ground and excited states of salicylic acid dimer. *J. Phys. Chem. A* **2006**, *110*, 12662–12669. [CrossRef] [PubMed]
61. Raeker, T.; Hartke, B. Full-Dimensional Excited-State Intramolecular Proton Transfer Dynamics of Salicylic Acid. *J. Phys. Chem. A* **2017**, *121*, 5967–5977. [CrossRef]
62. Suresh, S.; Gunasekaran, S.; Srinivasan, S. Spectroscopic (FT-IR, FT-Raman, NMR and UV-Visible) and quantum chemical studies of molecular geometry, Frontier molecular orbital, NLO, NBO and thermodynamic properties of salicylic acid. *Spectrochim. Acta A Mol. Biomol. Spectrosc.* **2014**, *132*, 130–141. [CrossRef]
63. Yu, J.; Su, N.Q.; Yang, W. Describing Chemical Reactivity with Frontier Molecular Orbitalets. *JACS* **2022**, *2*, 1383–1394. [CrossRef]
64. Ertl, P.; Gerebtzoff, G.; Lewis, R.; Muenkler, H.; Schneider, N.; Sirockin, F.; Stiefl, N.; Tosco, P. Chemical Reactivity Prediction: Current Methods and Different Application Areas. *Mol. Inform.* **2022**, *41*, 2100277. [CrossRef] [PubMed]
65. Kohn, W.; Becke, A.D.; Parr, R.G. Density functional theory of electronic structure. *J. Phys. Chem.* **1996**, *100*, 12974–12980. [CrossRef]

66. Domingo, L.R.; Aurell, M.J.; Pérez, P.; Contreras, R. Quantitative character-ization of the global electrophilicity power of common diene/dienophile pairs in Diels-Alder reactions. *Tetrahedron* **2002**, *58*, 4417–4423. [CrossRef]
67. Contreras, P.; Seijas, L.; Osorio, D. TDOS quantum mechanical visual analysis for single molecules. *Can. J. Pure Appl. Sci.* **2021**, *15*, 5239–5245.
68. Sjoberg, P.; Politzer, P. Use of the electrostatic potential at the molecular surface to interpret and predict nucleophilic processes. *J. Phys. Chem.* **1990**, *94*, 3959–3961. [CrossRef]
69. Politzer, P.; Laurence, P.R.; Jayasuriya, K. Molecular electrostatic potentials: An effective tool for the elucidation of biochemical phenomena. *Environ. Health Perspect.* **1985**, *61*, 191–202. [CrossRef]
70. Johnson, E.R.; Keinan, S.; Mori-Sánchez, P.; Contreras-García, J.; Cohen, A.J.; Yang, W. Revealing Noncovalent Interactions. *J. Am. Chem. Soc.* **2010**, *132*, 6498–6506. [CrossRef]
71. Hobza, P. Calculations on noncovalent interactions and databases of benchmark interaction energies. *Acc. Chem. Res.* **2012**, *45*, 663–672. [CrossRef]
72. Alqahtani, S. In silico ADME-Tox modeling: Progress and prospects. *Expert. Opin. Drug Metab. Toxicol.* **2017**, *13*, 1147–1158. [CrossRef]
73. Filho, R.P.; Polli, M.C.; Filho, S.B.; Garcia, M.; Ferreira, E.I. Prodrugs available on the Brazilian pharmaceutical market and their corresponding bioactivation pathways. *Braz. J. Pharm. Sci.* **2010**, *46*, 393–420. [CrossRef]
74. Montinari, M.R.; Minelli, S.; De Caterina, R. The first 3500 years of aspirin history from its roots—A concise summary. *Vascul. Pharmacol.* **2019**, *113*, 1–8. [CrossRef] [PubMed]